Nanoscale

Biomolecule Sensing by Surface Enhanced Raman Scattering of Monolayer Janus Transition Metal Dichalcogenide

Journal:	*Nanoscale*
Manuscript ID	NR-ART-01-2020-000300.R2
Article Type:	Paper
Date Submitted by the Author:	08-Apr-2020

Complete List of Authors:	Jia, Shuai; Rice University, Department of Materials Science and NanoEngineering Bandyopadhyay, Arkamita; University of Pennsylvania Kumar, Hemant; University of Pennsylvania, Materials Science and Engineering Zhang, Jing; Rice University, Materials Science and NanoEngineering Wang, Weipeng ; Tsinghua University, School of Materials Science & Engineering Zhai, Tianshu; Rice University Shenoy, Vivek; University of Pennsylvania, Department of Materials Science and Engineering Lou, Jun; Rice University, Department of Materials Science and NanoEngineering

Biomolecule Sensing by Surface Enhanced Raman Scattering of Monolayer Janus Transition Metal Dichalcogenide

Shuai Jia[1], Arkamita Bandyopadhyay[2], Hemant Kumar[2], Jing Zhang[1], Weipeng Wang[1], Tianshu Zhai[1], Vivek B. Shenoy[2], Jun Lou[1]*

1. *Department of Materials Science and NanoEngineering, Rice University, 6100 Main Street, Houston, TX 77005, USA*

2. *Department of Materials Science and Engineering, University of Pennsylvania, 3231 Walnut St, Philadelphia, PA 19104, USA*

Corresponding author: jlou@rice.edu (J. Lou)

Abstract

In this work, we demonstrate that monolayer Janus MoSSe is an effective and universal platform for enhancing Raman signal and detecting biomolecules for the first time. The out-of-plane dipoles in monolayer Janus MoSSe redistribute charges of adsorbed biomolecules, polarize biomolecules and enhance their Raman vibrational intensity. The estimated Raman enhancement factor is higher than 10^5, which is comparable with the highest reported enhancement factor for 2D substrates. The C-C stretching Raman peak around 1360 cm^{-1} is used to indicate glucose concentration and its peak-integrated intensity increases linearly with glucose concentration in the range of 1-10 mM. DFT calculation also confirms that charge redistribution in glucose induced by dipole interactions can enhance Raman intensity significantly when glucose molecule is adsorbed onto monolayer Janus MoSSe.

Introduction

Surface Enhanced Raman Scattering (SERS) has been widely investigated in the past several decades, for both fundamental studies of light-matter interaction and applications of microanalytical technique.[1–4] SERS is well known for its superior selectivity and excellent sensitivity towards target molecules, which originate from the substances' unique vibrational fingerprints and strong molecule-substrate or light-substrate interactions. These merits grant SERS the capability to sense trace amount of molecules or even single molecule, rendering it a promising analytical technique for sensing, health monitoring and in-situ dynamic tracking of catalytic process.[5–13] Importantly, optical detection methods are prompt-responsive and non-invasive, making them perfect tools for health monitor applications, such as saliva and sweat analysis.[14] Although this phenomenon is intensively studied, there are still many ambiguities, especially for the Raman enhancement mechanism. Generally, electromagnetic mechanism (EM) and chemical mechanism (CM) are the two mostly accepted origins for Raman signal enhancement. For EM, incident light generates surface plasmon and enhances local electromagnetic field among nanoscale metallic structures, such as gold particles and coper bowties.[1,15] On the other hand, CM is believed to involve charge transfer or dipole interactions between molecules and substrate, yet it is not well understood so far.[16] Discovery of new SERS media which subjects to CM may provide additional insight to help improve the understanding. Despite the huge enhancement factor usually observed for nanoscale metallic structure, side-reactions of adsorbates being catalyzed by these nanometallic structures are easy to happen in EM. The drawback of these side-reactions is that they generate a strong spectra background, which hinders the practical applications

of SERS. Therefore, exploring nonmetallic and SERS-active substrate is of critical importance for overcoming these disadvantages of nanometallic substrates.

Two-dimensional (2D) materials have attracted both academic and industrial interests and attentions in the past decade, because they exhibit novel electrical, mechanical, chemical, and thermal properties which are rare in their bulk counterparts.[17–23] Since the discovery of graphene in 2004, various other 2D materials have been synthesized successfully in recent years, including hexagonal boron nitride (h-BN), transition metal dichalcogenide (TMDs), MXene and many more in the rapidly growing 2D family.[24–28] Interestingly, a diverse set of 2D materials have been reported to exhibit Raman enhancement effect, including graphene, h-BN, and TMDs, and such effect is attributed to different enhancement mechanisms.[29–35] For instance, Raman enhancement effect in graphene depends on ground-state charge transfer interactions with adsorbates,[29] while h-BN utilizes interface dipole-dipole interactions to enhance Raman scattering.[31] However, the probe molecules that work with these nonmetallic substrate are limited to specific structures that possess large Raman scattering cross-section area in most cases, such as copper phthalocyanine (CuPc), rhodamine 6G (R6G) and protoporphyin IX(PPP).[29,31,33] This limitation makes it challenging to detect small biomolecules, that have significant value for health monitoring, e.g. glucose and dopamine sensing, using SERS with nonmetallic substrates, especially 2D materials.

Based on the dipole-dipole interaction mechanism, substrates that have effective out-of-plane dipoles have the highest chance to be SERS-active. Nevertheless, common 2D materials are crystals with highly symmetric structures in the out-of-plane direction, and they do not typically carry atomic-scale dipoles unless intendedly treated otherwise. Exceptions are distorted 1T' crystals including 1T'-WTe_2 and $MoTe_2$, which have been reported as SERS-active substrates.[36] Still, those distorted structures exhibit dipoles along specific in-plane directions. On the other hand, monolayer Janus transition metal dichalcogenide, e.g. Janus MoSSe, in which the tri-layer atomic structures from top to bottom are S, Mo and Se respectively, has been synthesized successfully recently by controlled sulfurization of chemical vapor deposition (CVD) grown monolayer $MoSe_2$.[37,38] Density functional theory (DFT) calculation has shown that the breaking of the out-of-plane symmetry structure could change electronic, mechanical and optical properties of monolayer TMDs dramatically.[39,40] More importantly, the asymmetrical structure also generates out-of-plane dipoles between the top S and bottom Se atoms, enabling strong interactions between the substrate with surrounding environment, as well as adsorbed molecules. With these factors considered, the dipole interactions from monolayer Janus MoSSe are highly promising for the enhancement of Raman scattering.

In the present work, we demonstrate that monolayer Janus MoSSe is an effective SERS platform for biomolecules sensing for the first time. Strong characteristic Raman peaks of glucose are observed from monolayer Janus MoSSe, because of the strong dipole interactions between probe molecules and the Janus substrate. The estimated Raman enhancement factor is higher than 10^5, which is comparable with the highest reported

Raman enhancement factor for 2D substrates.[35] In contrast, molybdenum disulfide (MoS_2) and molybdenum diselenide ($MoSe_2$), which are symmetric along out-of-plane direction, do not exhibit any obvious Raman enhancement for glucose. The C-C stretching Raman peak around 1360 cm^{-1} is used to indicate glucose concentration and its peak-integrated intensity increases linearly with glucose concentration in the range of 1-10 mM. DFT calculation also indicates that charge redistribution in glucose induced by dipole interactions could enhance Raman intensity significantly when glucose molecule is adsorbed onto monolayer Janus MoSSe. Our work opens a new direction to detect biomolecules using monolayer Janus TMDs as SERS-active substrate.

Results and Discussion

Monolayer Janus MoSSe was synthesized by a controlled surface-limited sulfurization process, which was described in our previous work.[37] Specifically, sulfur atoms replaced exclusively the whole layer of selenium atoms on the top side of a CVD-grown monolayer $MoSe_2$ to build this sandwiched S-Mo-Se structure of the Janus MoSSe, which is shown in Figure 1. The triangular shapes of the single-crystalline monolayer flakes were retained after the surface sulfurization. Despite the change in optical color contrast in Janus MoSSe compared with original $MoSe_2$ on SiO_2 substrate, which originates from a bandgap shift, these flakes remain clearly visible. This makes it easy to observe and inspect the same piece of material for SERS under different glucose concentrations. Two typical characteristic vibrational modes that are usually observed in TMDs, namely, A_{1g} for out-of-plane vibration and E_{2g} for in-plane vibration, were clearly

observed in the Raman spectra of Janus MoSSe at 290 and 350 cm^{-1} respectively.[37] In Janus MoSSe, the structural out-of-plane symmetry is broken, granting this artificial material properties that do not exist in nature. For instance, large out-of-plane piezoelectric polarization in monolayer Janus could be induced by a uniaxial strain in the basal plane, revealing the potential to utilize piezoelectric 2D materials in device applications.[39]

Dipoles aligned along the out-of-plane direction were generated in monolayer Janus because of the asymmetric S-Mo-Se sandwiched structure and different electronegativity in top S and bottom Se atoms. These aligned dipoles in Janus MoSSe reach out to interact actively with surrounding dipoles in adsorbates. Raman spectrum was collected and compared to trace the dipole-dipole interactions between monolayer Janus and adsorbates. Here we used glucose, which was one of the most important metabolites for human, as the probe molecule. A droplet of glucose solution was dropped on top of 2D TMDs on SiO_2 substrate. Raman spectra were collected on monolayer MoS_2 or $MoSe_2$ or Janus MoSSe after the substrate was air-dried. No obvious peaks of glucose were observed on monolayer MoS_2 or $MoSe_2$ (Figure S2 in supporting information), which excluded the potential SERS activity originating from Mo-based TMDs in their natural 2H configuration. However, multiple strong Raman peaks appeared on monolayer Janus MoSSe loaded with glucose with 532 nm laser (Figure 2c and Figure S3). This was in line with our expectation, that dipole-dipole interaction was significant between monolayer Janus MoSSe and glucose, and the interaction enhanced glucose's vibrational intensity markedly. The magnification of vibration boosted the sensitivity of SERS by

monolayer Janus MoSSe, enabling the detection of glucose at concentration as low as 500 μM. In contrast, due to the lack of aforementioned dipoles in MoS_2 or $MoSe_2$, the interaction between these materials and glucose was very weak and did not promote any Raman enhancement effect for the probe molecule. This suggests monolayer Janus MoSSe is SERS-active for small biomolecules.

To observe the enhancement of Raman peaks clearly, a differential was applied to original Raman spectra of glucose on monolayer Janus MoSSe (Figure 2d). The main peaks were located around 772 cm^{-1}, 928 cm^{-1}, 993 cm^{-1}, 1180 cm^{-1}, 1311 cm^{-1}, 1360 cm^{-1}, which were identified as C rocking, C ring breathing, C ring distortion, C-O-C bending, C-O stretching, C-C stretching, respectively, and were consistent with Raman peaks of glucose powder (Table S1 in supporting information).[41] Two enhanced peaks of glucose located at ~ 928 cm^{-1} and 993 cm^{-1} overlapped with the strong and wide background peak of silicon at 900-1050 cm^{-1} (Figure 2c). However, they were clearly observed in the differential spectra (Figure 2d). It is worth noting that not all the vibrational modes in glucose powder were clearly observed on the wide Raman spectra of glucose on monolayer Janus MoSSe. The first reason is that multiple peaks in SERS were broadened and aggregated to form a wide background. Careful deconvolution is needed to identify these hidden peaks. The second reason is that various adsorption configurations of glucoses on monolayer Janus MoSSe might coexist, resulting in different enhancement effects for various glucose molecules adsorbed on Janus MoSSe. The third reason is that the enhancement effects for various vibrational modes in glucose are different even for

same adsorption configuration of glucose on Janus MoSSe. This is because the Raman enhancement comes from dipole-dipole interactions of glucose and Janus, which depends on vibrational orientations in glucose. Different vibrational modes in glucose, like C-C stretching, C-O stretching, have different orientations, resulting in different interactions and Raman enhancement effects. In other words, the aligned dipoles in Janus interacted differently with various vibrational modes in glucose. As a result, not all glucose peaks were observed on monolayer Janus MoSSe.

It is worthwhile to note that we did not see any obvious peak on blank SiO_2/Si substrate, and the Raman enhancement factors could not be calculated directly. To estimate the Raman enhancement factor for glucose on monolayer Janus MoSSe, a thick layer of glucose powder was directly put on blank SiO_2/Si substrate for Raman measurement. Its Raman spectra is shown in Figure 3 and its Raman intensity could be described by equation 1. On the other hand, a droplet of 10 mM glucose solution with volume of 50 μL was dropped on monolayer Janus substrate. Raman spectrum was collected after substrate was blow-dried. Here we assumed all the glucose molecules were adsorbed on the substrate, and the absorption of glucose on the entire substrate was uniform. Its Raman intensity was represented by equation 2. The calculated enhancement factor was about $4x10^5$, which was comparable with that of EM with nanometallic substrates.[1,31,32] Please note that this is a very conservative estimation for Raman enhancement factor because only small part of glucose molecules in the droplet were adsorbed on Janus substrate.

$$\frac{N_{blank}}{S_{blank}} * S_{laserspot} * I_0 = I_{blank} \quad (1)$$

$$\frac{N_{Janus}}{S_{Janus}} * S_{laserspot} * I_0 * E = I_{Janus} \quad (2)$$

$$E = \frac{I_{Janus} N_{blank} S_{Janus}}{I_{blank} S_{blank} N_{Janus}} \quad (3)$$

Where, N_{blank} is the number of glucose molecules on blank substrate (SiO_2/Si here). S_{blank} is the area of blank SiO_2/Si substrate. $S_{laserspot}$ is the spot size of laser for Raman measurement. I_0 is the vibrational intensity of single glucose molecule. I_{blank} is the integrated Raman intensity for peak at 1360 cm^{-1} on blank SiO_2/Si substrate. N_{Janus} is the number of glucose molecules on Janus substrate, and could be achieved by the concentration and volume dropped on Janus substrate. E is the enhancement factor, I_{Janus} is the integrated Raman intensity for peak at 1360 cm^{-1} on Janus substrate.

A series of glucose solutions with various concentrations were prepared to test the Raman enhancement responses. To be consistent, all the monolayer Janus substrate (monolayer Janus samples/SiO_2/Si) used here had almost the same area and came from same batch of synthesis with almost the same TMDs area coverage everywhere. Importantly, the Raman peak intensity increased with elevated glucose concentration (Figure 4a). The C-C stretching peak around 1360 cm^{-1} was selected as the indicator, since it had the highest sensitivity towards variation in glucose concentration in our test. Its integrated peak intensity increased linearly with glucose concentration in the range of 1-10 mM (Figure 4b). When glucose concentration was higher than 10 mM, its peak-integrated intensity began to deviate from the linear projection. This might be due to that few-layers glucose began to adsorb on Janus MoSSe for high concentration solutions, resulting in different dipole interaction and Raman enhancement effect. This linear correlation of Raman

intensity and glucose concentration (in the range of 1-10 mM) makes monolayer Janus MoSSe an excellent substrate for biomolecules sensing and takes a step forward of the practical application of SERS technique-based health monitoring.

DFT calculations were also performed to provide insights into the interactions of monolayer Janus MoSSe and glucose. Theoretical calculation shows the valance band (VB) and conduction band (CB) of monolayer Janus are around -5.8 and -4.3 eV, respectively. The highest occupied molecular orbital (HOMO) and lowest unoccupied molecular orbital (LOMO) level of glucose molecule are around -5.65 and -0.82 eV. The potential charge transfer paths, including from Janus MoSSe VB to glucose LOMO, Janus MoSSe CB to glucose LOMO and glucose HUMO to Janus CB, all have high energy barriers, resulting in low charge transfer probability. This excludes the charge transfer as the main approach to enhance Raman signal of adsorbed glucose molecules. To explore dipole interaction effect on Raman enhancement, different configurations of glucose adsorption onto monolayer Janus MoSSe were considered (Figure S5 in supporting information). The first configuration, in which the CH_2OH group of glucose pointed away from the surface, was found to be the most stable one (-0.8 eV). This stable structure was used to calculate charge distribution and Raman spectra in the complex. The calculated out-of-plane dipole moment in monolayer Janus is as high as + 0.33 eÅ, resulting in charge redistribution in glucose molecules by a proximity effect, which in turn, led to polarization of dipole in the molecule and enhancement of Raman intensity. The positive sign here in the dipole of monolayer Janus MoSSe meant its direction was pointed out from bottom Se to top S. The charge redistribution plot in isolated glucose

molecule (the light blue electron cloud density as depicted in Figure 5a) vs. absorbed glucose molecule onto monolayer Janus (the purple electron density), showed significant amount of charge redistribution in glucose because of a strong surface-molecule interaction with monolayer Janus MoSSe. This charge redistribution changed the dipole of glucose from -0.05 eÅ to 0.23 eÅ. The Raman intensity of glucose also increased significantly when the glucose and Janus composite structure was considered (Figure 5b). However, different Raman vibrational modes showed various enhancement effects. Note that the charge redistribution depended on the molecular configuration on Janus surface and as a result, the change of dipole moment did not have the same amplitude for all atoms or bonds. Thus, different Raman modes of glucose showed different enhancement effects.

Attractively, SERS effect originating from monolayer Janus MoSSe is potentially universal to a wide variety of biomolecules. Dopamine, a hormone functioning as a neurotransmitter, plays several important roles in human brain and body. Its Raman spectra was also detected here with monolayer Janus MoSSe as the substrate. As shown in Figure 3b, two wide and strong peaks located at 1451 and 1553 cm^{-1}, corresponding to C ring vibrational modes, were observed in the Raman spectra. Similarly, charge redistribution induced by strong interactions between monolayer Janus MoSSe and dopamine would polarize dipoles in the probe molecule and enhance their Raman intensity. This interesting universality of dipole interaction makes our monolayer Janus substrate promising for the detection of complex target containing multiple molecules.

Conclusions

In summary, monolayer Janus MoSSe, as an effective and universal SERS-active substrate for detecting biomolecules, was demonstrated for the first time. The out-of-plane dipole in monolayer Janus MoSSe redistributed charges and, polarized dipoles in biomolecules such as glucose and dopamine, and enhanced their Raman vibrational intensity as verified by corresponding DFT calculations. The estimated Raman enhancement factor is higher than 10^5. The universality of interaction between monolayer Janus MoSSe and biomolecules makes Janus a useful substrate for Raman enhancement that can be adapted for sensing of other molecules. Our finding not only provides new insight into the dipole interactions between monolayer Janus TMDs and molecules, as well as CM process in SERS, but also paves the way for future applications of 2D materials-based SERS sensing and detection technique.

Experimental

Preparation of monolayer Janus MoSSe:

Monolayer $MoSe_2$ was firstly grown on SiO_2/Si substrate with conventional CVD method. A facile sulfurization process was utilized to convert $MoSe_2$ to Janus MoSSe. Briefly, sulfur powder (Sigma-Aldrich) was placed at upstream of a heating zone of a tube furnace and heated up to 150℃ to generate sulfur vapor. The heated sulfur vapor was introduced into tube center by argon as carrier gas. Conversion from $MoSe_2$ to Janus MoSSe was triggered by the selective substitution of top layer of selenium by sulfur.[37]

This furnace was kept at 800℃ for 30 mins before cooling down to room temperature naturally.

Preparation and characterization of SERS samples

Glucose powder (Sigma-Aldrich), was dissolved into deionized water to prepare solution with various concentrations. To rule out the batch to batch difference, all the Janus samples used for linear concentration range calibration came from the same big substrate, which was cut into small pieces (~5*5mm^2). A drop, whose volume was about 50uL, was dropped onto substrate with dense monolayer Janus flakes. The substrate was then blow-dried with an air gun. Raman spectra was collected in Renishaw confocal microscope with 532 nm excitation laser.

DFT calculation

We have performed DFT calculations using the Vienna Ab-Initio Simulation Package (VASP) with projector-augmented wave (PAW) pseudopotentials and the Perdew−Burke −Ernzerhof (PBE) exchange-correlation functional. We have used a 6 × 6 × 1 Janus MoSSe surface and 25 Å vacuum in the z-direction to avoid all spurious interactions between the adsorbed glucose molecules. A plane-wave basis set energy cutoff of 400 eV was used for the surface and surface-molecule composite optimization and the forces on each atom were converged to less than 0.01 eV/Å. The total energy changes were converged to less than 10^{-8} eV. We have used a Γ-centered k-point mesh of 9 × 9 × 1 for ground state calculations as well as Γ-centered phonon mode calculation.

Acknowledgments:

The authors gratefully acknowledge the support by the Welch grant C-1716 and the NSF I/UCRC Center for Atomically Thin Multifunctional Coatings (ATOMIC) under award # IIP-1539999.

References

1 S.-Y. Ding, J. Yi, J.-F. Li, B. Ren, D.-Y. Wu, R. Panneerselvam and Z.-Q. Tian, *Nat. Rev. Mater*, 2016, **1**, 16021.

2 M. F. Cardinal, E. Vander Ende, R. A. Hackler, M. O. McAnally, P. C. Stair, G. C. Schatz and R. P. Van Duyne, *Chem. Soc. Rev.*, 2017, **46**, 3886–3903.

3 S. Schlücker, *Angew. Chem. Int. Edi.*, 2014, **53**, 4756–4795.

4 B. Sharma, R. R. Frontiera, A. I. Henry, E. Ringe and R. P. Van Duyne, *Mater. Today*, 2012, **15**, 16–25.

5 O. Lyandres, J. M. Yuen, N. C. Shah, R. P. VanDuyne, J. T. Walsh and M. R. Glucksberg, *Diabetes Technol. Ther.*, 2008, **10**, 257–265.

6 C. Y. Song, Y. J. Yang, B. Y. Yang, Y. Z. Sun, Y. P. Zhao and L. H. Wang, *Nanoscale*, 2016, **8**, 17365–17373.

7 J. Kneipp, *ACS Nano*, 2017, **11**, 1136–1141.

8 E. C. Lin, J. Fang, S. C. Park, F. W. Johnson and H. O. Jacobs, *Nat. Commun.*, 2013, **4**, 1636–1638.

9 A. F. Palonpon, J. Ando, H. Yamakoshi, K. Dodo, M. Sodeoka, S. Kawata and K. Fujita, *Nat. Protoc.*, 2013, **8**, 677–692.

10 F. Sun, H.-C. Hung, A. Sinclair, P. Zhang, T. Bai, D. D. Galvan, P. Jain, B. Li, S. Jiang and Q. Yu, *Nat. Commun.*, 2016, **7**, 13437.

11 Y. Hu, H. Cheng, X. Zhao, J. Wu, F. Muhammad, S. Lin, J. He, L. Zhou, C. Zhang, Y. Deng, P. Wang, Z. Zhou, S. Nie and H. Wei, *ACS Nano*, 2017, **11**, 5558–5566.

12 H. Zhang, C. Wang, H.-L. Sun, G. Fu, S. Chen, Y.-J. Zhang, B.-H. Chen, J. R. Anema, Z.-L. Yang, J.-F. Li and Z.-Q. Tian, *Nat. Commun.*, 2017, **8**, 15447.

13 Y. Su, S. Jia, J. Du, J. Yuan, C. Liu, W. Ren and H. Cheng, *Nano Res.*, 2015, **8**, 3954–3962.

14 R. Pandey, S. K. Paidi, T. A. Valdez, C. Zhang, N. Spegazzini, R. R. Dasari and I. Barman, *Acc. Chem. Res.*, 2017, **50**, 264–272.

15 W. Xu, X. Ling, J. Xiao, M. S. Dresselhaus, J. Kong, H. Xu, Z. Liu and J. Zhang, *Proc. Nat. Aca. Sci.*, 2012, **109**, 9281–9286.

16 A. Otto, *J. Raman. Spectrosc*, 2005, **36**, 497–509.

17 Y. Shi, H. Li and L.-J. Li, *Chem. Soc. Rev.*, 2015, **44**, 2744–2756.

18 R. Lv, J. A. Robinson, R. E. Schaak, D. Sun, Y. Sun, T. E. Mallouk and M. Terrones, *Acc. Chem. Res.*, 2015, **48**, 56–64.

19 G. R. Bhimanapati, Z. Lin, V. Meunier, Y. Jung, J. Cha, S. Das, D. Xiao, Y. Son, M. S. Strano, V. R. Cooper, L. Liang, S. G. Louie, E. Ringe, W. Zhou, S. S. Kim, R. R. Naik, B. G. Sumpter, H. Terrones, F. Xia, Y. Wang, J. Zhu, D. Akinwande,

N. Alem, J. A. Schuller, R. E. Schaak, M. Terrones and J. A. Robinson, *ACS Nano*, 2015, **9**, 11509–11539.

20 T. Heine, *Acc. Chem. Res.*, 2015, **48**, 65–72.

21 Y. Wang, N. Xu, D. Li and J. Zhu, *Adv. Funct. Mater.*, 2017, **19**, 1604134.

22 B. Radisavljevic, A. Radenovic, J. Brivio, V. Giacometti and A. Kis, *Nat Nanotechnol*, 2011, **6**, 147–150.

23 Z. Jin, F. Ye, X. Zhang, S. Jia, L. Dong, S. Lei and R. Vajtai, *ACS Nano*, 2018, **12**, 12571–12577.

24 X. Li, W. Cai, J. An, S. Kim, J. Nah, D. Yang, L. Colombo and R. S. Ruoff, *Science.*, 2009, **3893**, 1312–1315.

25 G. Lu, T. Wu, Q. Yuan, H. Wang, H. Wang, F. Ding, X. Xie and M. Jiang, *Nat. Commun.*, 2015, **6**, 6160.

26 G. Lu, T. Wu, P. Yang, Y. Yang, Z. Jin, W. Chen, S. Jia, H. Wang, G. Zhang, J. Sun, P. M. Ajayan, J. Lou, X. Xie and M. Jiang, *Adv. Sci.*, 2017, **4**, 1–7.

27 S. Najmaei, Z. Liu, W. Zhou, X. Zou, G. Shi, S. Lei, B. I. Yakobson, J.-C. Idrobo, P. M. Ajayan and J. Lou, *Nat. Mater.*, 2013, **12**, 754–759.

28 H. Wang, Y. Wu, X. Yuan, G. Zeng, J. Zhou, X. Wang and J. W. Chew, *Adv. Mater.*, 2018, **1704561**, 1–28.

29 X. Ling, L. Xie, Y. Fang, H. Xu, H. Zhang, J. Kong, M. S. Dresselhaus, J. Zhang and Z. Liu, *Nano Lett*, 2010, **10**, 553–561.

30 D. Liu, X. Chen, Y. Hu, T. Sun, Z. Song, Y. Zheng, Y. Cao, Z. Cai, M. Cao, L. Peng, Y. Huang, L. Du, W. Yang, G. Chen, D. Wei, A. T. S. Wee and D. Wei, *Nat. Commun.*, 2018, **9**, 1–10.

31 X. Ling, W. Fang, Y. H. Lee, P. T. Araujo, X. Zhang, J. F. Rodriguez-Nieva, Y. Lin, J. Zhang, J. Kong and M. S. Dresselhaus, *Nano Lett*, 2014, **14**, 3033–3040.

32 Y. Tan, L. Ma, Z. Gao, M. Chen and F. Chen, *Nano Lett*, 2017, **17**, 2621–2626.

33 Z. Zheng, S. Cong, W. Gong, J. Xuan, G. Li, W. Lu, F. Geng and Z. Zhao, *Nat. Commun.*, 2017, **8**, 2–11.

34 Y. Yin, P. Miao, Y. Zhang, J. Han, X. Zhang, Y. Gong, L. Gu, C. Xu, T. Yao, P. Xu, Y. Wang, B. Song and S. Jin, *Adv. Funct. Mater.*, 2017, **27**, 1606694.

35 C. Muehlethaler, C. R. Considine, V. Menon, W. Lin, Y. Lee and J. R. Lombardi, *ACS Photonics*, 2016, **3**, 1164–1169.

36 L. Tao, K. Chen, Z. Chen, C. Cong, C. Qiu and J. Chen, *J. Am. Chem. Soc.*, 2018, **140**, 8696–8704.

37 J. Zhang, S. Jia, I. Kholmanov, L. Dong, D. Er, W. Chen, H. Guo, Z. Jin, V. B. Shenoy, L. Shi and J. Lou, *ACS Nano*, 2017, **11**, 8192–8198.

38 A.-Y. Lu, H. Zhu, J. Xiao, C.-P. Chuu, Y. Han, M.-H. Chiu, C.-C. Cheng, C.-W. Yang, K.-H. Wei, Y. Yang, Y. Wang, D. Sokaras, D. Nordlund, P. Yang, D. A. Muller, M.-Y. Chou, X. Zhang and L.-J. Li, *Nat. Nanotechnol.*, 2017, 1–29.

39 L. Dong, J. Lou and V. B. Shenoy, *ACS Nano*, 2017, **11**, 8242–8248.

40 J. Wang, H. Shu, T. Zhao, P. Liang, N. Wang, D. Cao and X. Chen, *Phys. Chem. Chem. Phys*, 2018, **20**, 18571–18578.

41 B. Sharma, P. Bugga, L. R. Madison, A. I. Henry, M. G. Blaber, N. G. Greeneltch, N. Chiang, M. Mrksich, G. C. Schatz and R. P. Van Duyne, *J. Am. Chem. Soc.*, 2016, **138**, 13952–13959.

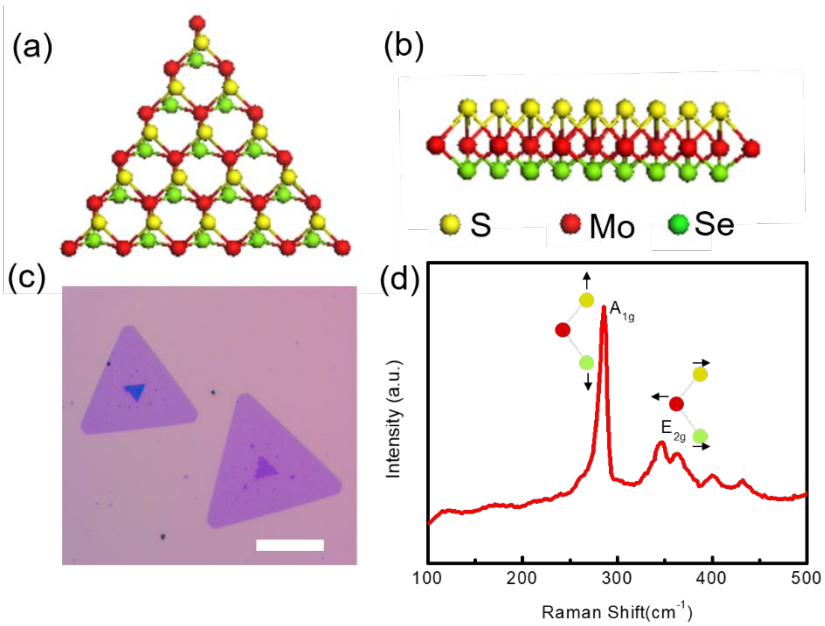

Figure 1. Schematic illustration of monolayer Janus MoSSe. (a-b). Top-view and front-view of monolayer Janus MoSSe. (c) Optical image of monolayer Janus MoSSe. The scale bar is 20 μm. (d) Typical Raman spectrum of monolayer Janus MoSSe.

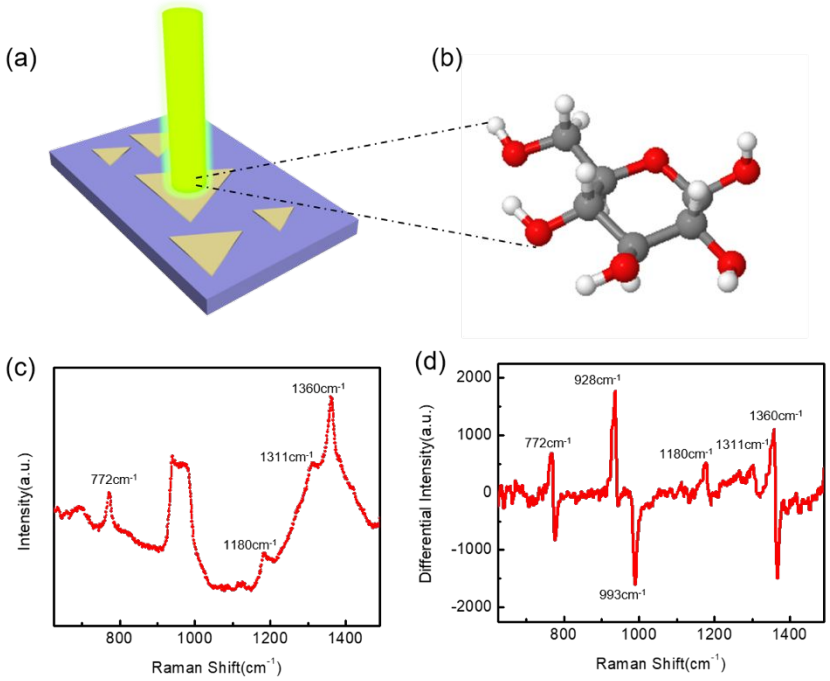

Figure 2. (a) Schematics of laser irradiation of glucose on Janus MoSSe for SERS characterization. (b) Structure of adsorbed glucose molecule in (a). (c) Raman spectra of glucose absorbed onto monolayer Janus MoSSe. Multiple Raman peaks were enhanced by strong dipole interactions between glucose and Janus MoSSe. (d) Differential intensity of pristine Raman spectra in (c) showing characteristic Raman vibrational peaks clearly.

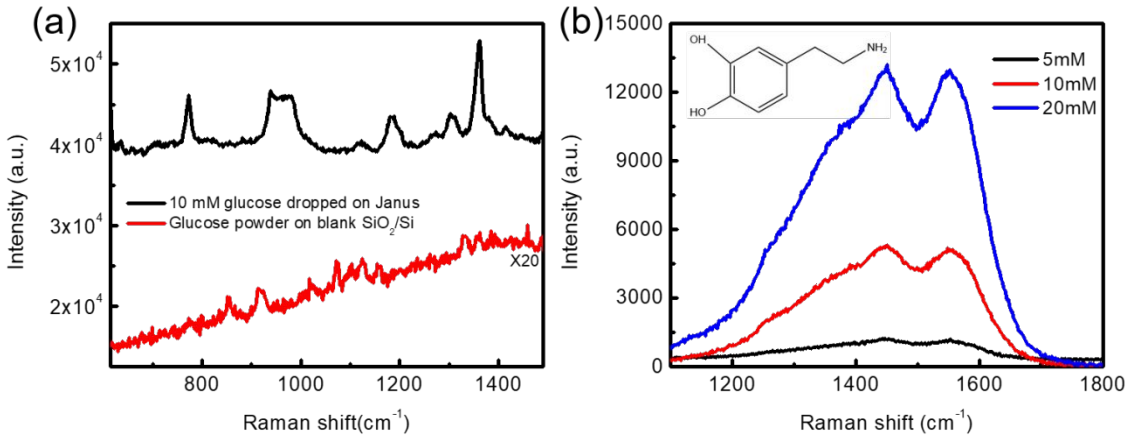

Figure 3. (a) Raman spectra of solid glucose powder on blank SiO_2/Si substrate and 10 mM glucose solution dropped on monolayer Janus MoSSe substrate. (b) Enhanced Raman spectra of dopamine solution dropped on monolayer Janus MoSSe substrate.

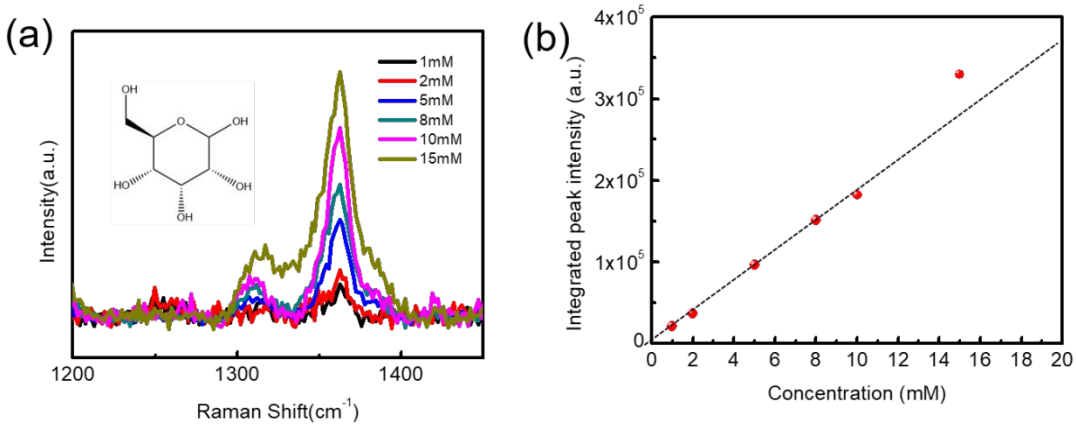

Figure 4. (a) Concentration-dependent Raman spectra of glucose on monolayer Janus MoSSe. The integrated peak intensity increased linearly with elevated glucose concentration in solution. (b) The calibration line obtained from the integrated peak intensity at 1360 cm^{-1} in (a). Integrated peak intensity begins to deviate from linear projections when concentration is higher than 10 mM.

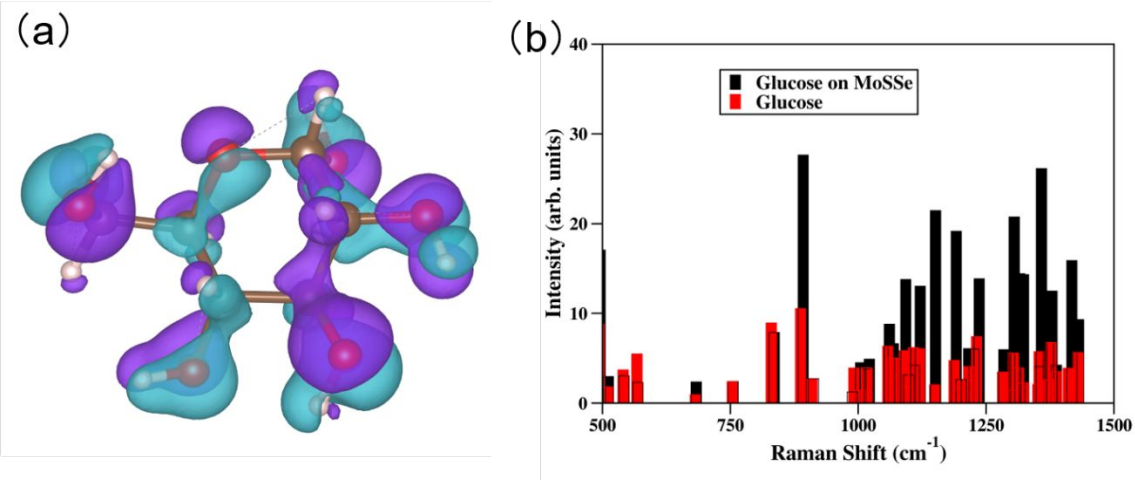

Figure 5. DFT calculations for the glucose molecule on monolayer Janus substrate. (a) Charge distribution in glucose. The light blue and the purple regions show the electron cloud distribution in isolated single glucose molecule and anchored glucose on monolayer Janus MoSSe, respectively. Their distinguishing shapes indicate the drastic charge redistribution after glucose is adsorbed on monolayer Janus MoSSe. (b) Calculated Raman peaks for isolated glucose and anchored glucose on Janus MoSSe.